Special Issue: Positioning of Tissue Engineering in Regenerative Medicine

Original Article

Ultrastructure of bone tissue ectopically regenerated by biodegradable hydrogels incorporating bone morphogenetic protein 2

Masaya Yamamoto, Yoshito Ikada and Yasuhiko Tabata*

Institute for Frontier Medical Sciences, Kyoto University, Kyoto, Japan

To study the ultrastructure of regenerated bone, the ectopically formed bone induced by gelatin hydrogels incorporating bone morphogenetic protein 2 (BMP-2) was evaluated through transmission electron microscopic (TEM) analyses including bright field electron imaging, selected area diffraction (SAD) imaging, and dark field electron imaging. After 2 weeks of implantation, ectopic bone induction was apparent at Wistar rat thigh muscles receiving the hydrogels incorporating BMP-2 through soft X-ray observation. The specimens for TEM study were prepared with an anhydrous method using ethylene glycol to maintain the structure of hydroxyapatite crystals. TEM observation of unstained ectopic bone cross-sections showed that electron dense substances were deposited on the gap zone of collagen fibers (intrafibrillar crystallites), while needle-like electron dense substances were observed in the intermolecular space of collagen fiber (extrafibrillar crystallites). SAD patterns suggested that these electron dense substances were hydroxyapatite crystals. Furthermore, from the SAD pattern and dark field electron image of intrafibrillar crystallites, it was presumed that the crystallographic c-axis of apatite crystals oriented to the direction of collagen fibril.

Rec.12/17/2013, Acc.12/19/2013, pp56-63

* Correspondence should be addressed to:
Yasuhiko Tabata, Institute for Frontier Medical Sciences, Kyoto University, 53 Kawahara-cho Shogoin, Sakyo-ku, Kyoto 606-8507, Japan. Phone: +81(75)751-4121, Fax: +81(75)751-4646, E-mail: yasuhiko@frontier.kyoto-u.ac.jp

Key words ectopic bone formation, collagen fibril, hydroxyapatite, crystallographic analysis, bone regeneration

Introduction

Biological tissues have excellent mechanical properties compared with artificial materials. A typical example is bone. However, biomaterials currently available for bone substitute have poor mechanical properties compared with those of the natural bone[1]. As the alternative treatment of bone reconstruction to tackle the mechanical incompatibility, bone regeneration has attracted much attention in the field of tissue engineering. A promising way to induce the regeneration of autologous osseous tissues in a bone defect

is to make use of bone-related growth factors, such as transforming growth factor-β1, basic fibroblast growth factor, and BMP[2-6]. We have reported that the controlled release of BMP-2 from a biodegradable hydrogel of gelatin with an isoelectric point (IEP) of 9.0 could enhance bone regeneration *in vivo* comparing with free BMP-2[7-9].

High toughness of the bone is due to the exquisite composite structure of collagen and hydroxyapatite (HAp). The crystallographic texture of HAp has been analyzed through X-ray diffraction[10-13], small angle X-ray scattering[14-16], neutron diffraction[17,18], synchrotron diffraction[19], Fourier transform infrared spectroscopy and microspectroscopy[20, 21], and Raman spectroscopy[22, 23], while X-ray diffraction[12], polarized light microscopy[24, 25], and Raman spectroscopy[26] have been utilized for analyzing collagen. We have developed a method to investigate the correlation between the crystallographic texture and the mechanical property of regenerated bone by combining microbeam X-ray diffraction (μXRD)[27-30] and nanoindentation mechanical testing[31]. Based on these studies, it is becoming evident that not only in normal bone but also in regenerated bone, the preferential orientation of HAp c-axis significantly contributes to the mechanical property.

On the contrary, the ultrastructural feature of mineralized tissues, such as tendon, bone and dentin, has been studied by use of various methods including conventional and high voltage electron microscopies[33-47] and tomography at the electron microscopic level[48-56], immunocytochemistry[57, 58], and atomic force microscopy[35, 56]. Most of these studies use a mineralized turkey leg tendon as a model of mineralized tissues, because of its high degree of collagen fibril alignment, thereby permitting the ease of sequential analyses in the mineralization process. However, the ultrastructural feature, which could affect the function of regenerated bone, has not been investigated.

The objective of this study is to investigate the ultrastructure of regenerated bone induced by gelatin hydrogels incorporating BMP-2. The ultrastructure of bone ectopically formed by the hydrogel incorporating BMP-2 was evaluated in terms of the collagen-mineral structure described in the mineralized turkey leg tendon. An anhydrous method with ethylene glycol and unstained cross-sections were employed for TEM analyses of regenerated bones in order to minimize the artifacts in HAp crystals caused by aqueous buffer solutions[46]. The mineralized collagen could be appeared on the electron microscopic image due to the electron dense feature of HAp. A crystallographic analysis combined with dark field electron imaging was performed to demonstrate the collagen-mineral structure in the ectopic bone.

Materials and Methods

1)Materials

BMP-2 was supplied by Yamanouchi Pharmaceutical Co., Tokyo, Japan. Gelatin was isolated from porcine skin through an acidic process with an IEP of 9.0 and an average molecular weight of 99,000 (Nitta Gelatin Co., Osaka, Japan). Other chemicals were obtained from Wako Pure Chemical Industries, Osaka, Japan and used without further purification.

2)Preparation of gelatin hydrogels

Gelatin hydrogels were prepared by chemical cross-linking of gelatin with glutaraldehyde[7-9]. Briefly, 4.29 wt% aqueous solution of gelatin (35 ml) was mixed with 2.17 wt% of glutaraldehyde (GA) aqueous solution (15 ml), and the resulting solution was cast into a polypropylene dish of 138 x 138 cm^2 and 5 mm depth, followed by leaving at 4℃ for 12 hr for gelatin crosslinking. The resulting hydrogel was punched out to obtain gelatin hydrogel discs (5 mm diameter and 2 mm thickness). Then, the hydrogel discs were placed in 100 mM glycine aqueous solution at 37℃ for 1 hr to block residual aldehyde groups of glutaraldehyde, followed by washing 3 times at 37℃ with double-distilled water. Finally, they were freeze-dried and sterilized with ethylene oxide gas. The weight percentage of water in the wet hydrogel was determined from the hydrogel weight measured before and after drying at 70℃ under vacuum for 6 hr. The water content of the hydrogel was approximately 97.8 wt%[7-9].

3)Implantation of gelatin hydrogels incorporating BMP-2

An aqueous solution of BMP-2 (0.5 mg / ml, 10 μl) was added to freeze-dried gelatin hydrogels to amount to 5 μg per each hydrogel. The gelatin hydrogel incorporating BMP-2 was allowed to stand at 4℃ for 12 hr before implantation. The hydrogel incorporating BMP-2 was implanted aseptically into the left thigh muscle of three 7-week-old male Wistar rats. After 2 weeks of implantation, the legs were examined by soft x-rays generated from Hitex HX-100, Hitachi, Japan, at a generator tension of 46 KVP and a current of 2.5 mA for 15 sec.

4)TEM observation

The tissue from the implant site was explanted for TEM evaluation. The explanted specimens were divided into two groups for the following treatment: group 1 was fixed with 2.5 wt% GA in 0.1 M phosphate buffer (PB, pH 7.4) at 4℃ for 1 hr and postfixed with 1 wt% osmium tetroxide in 0.1 M PB containing 0.1 M sucrose at 4℃ for 2 hr (aqueous preparation). Group 2 was treated with 100 % ethylene glycol at 4℃ for 24 hr under vacuum state (anhydrous preparation)[46]. The fixed specimens in group 1 were dehydrated in an ascending series of ethanol and placed in propylene oxide and subsequently in propylene oxide and an Epon resin mixture at room temperature. Then, the specimens in group 1 were soaked in the Epon resin under vacuum and embedded in the Epon resin. On the other hand, the specimens in group 2 were immersed in 2-ethoxyethanol at 4℃ for 24 hr under vacuum and placed in propylene oxide and the Epon resin mixture. Finally, the specimens in group 2 were embedded in the Epon resin. An ultrathin cross-section of 70 nm thickness was cut with an ultramicrotome from the formed bone tissue in both groups 1 and 2. The cross-sections were stained with both lead citrate and uranyl acetate, or unstained with any chemicals.

Bright field electron imaging was performed for both stained and unstained sections with TEM (JEM 1200EX II, JEOL, Tokyo, Japan) operating at 80 kV. Furthermore, the unstained specimen treated with the anhydrous preparation was investigated by selected area diffraction (SAD) combined with selected area dark field electron imaging under the same TEM condition as the bright field electron imaging.

Results

1)Bright field electron imaging of stained and unstained cross-sections

Soft x-ray observation showed that a radiopaque area could be seen at the leg receiving gelatin hydrogels incorporating BMP-2 after 2 weeks of implantation[7] (data not shown). Figures 1 and 2 show the bright field electron image of stained cross-sections for the ectopic bone treated with the aqueous and anhydrous preparations, respectively. As seen in Figure 1, osteoblasts actively produced an extracellular matrix containing collagen fibers, which were partially mineralized. Collagen fibers with a fine structural periodic banding of 64 nm and partial mineralization are seen in Figure 2[56-58].

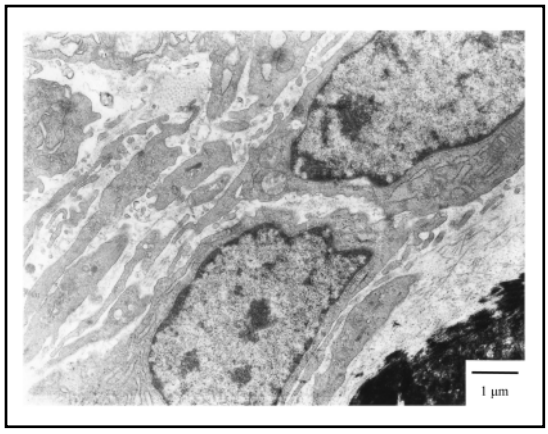

Fig.1 Bright field electron image of stained ectopic bone cross-section prepared through the aqueous method.

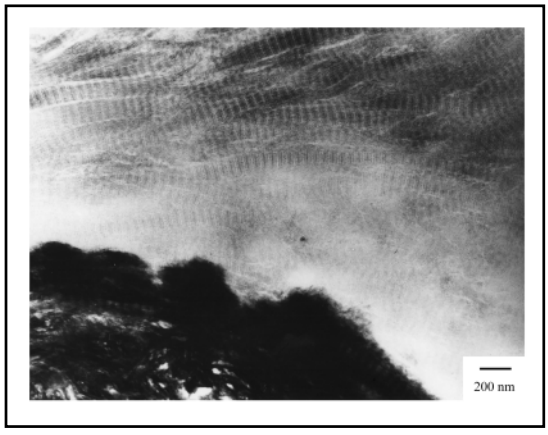

Fig.2 Bright field electron image of stained ectopic bone cross-section prepared through the anhydrous method.

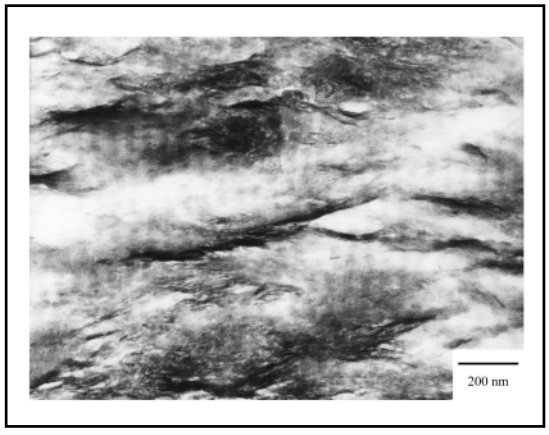

Fig.3 Bright field electron image unstained ectopic bone cross-section prepared through the anhydrous method.

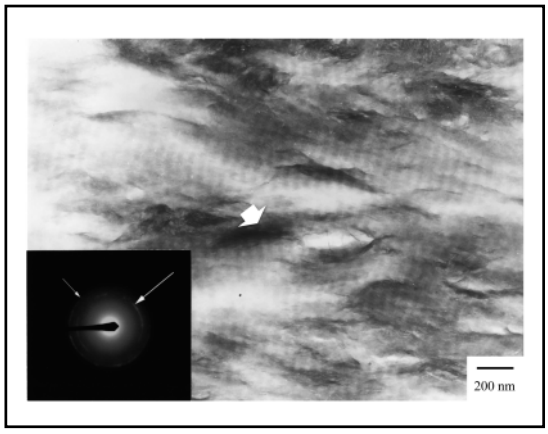

Fig.4 Bright field electron and SAD images of unstained ectopic bone cross-section prepared through the anhydrous method
Heavy arrow indicates the area of extrafibrillar crystallites used for the SAD image. The large and small arrows in the SAD image correspond to (002) and (211) lattice planes, respectively.

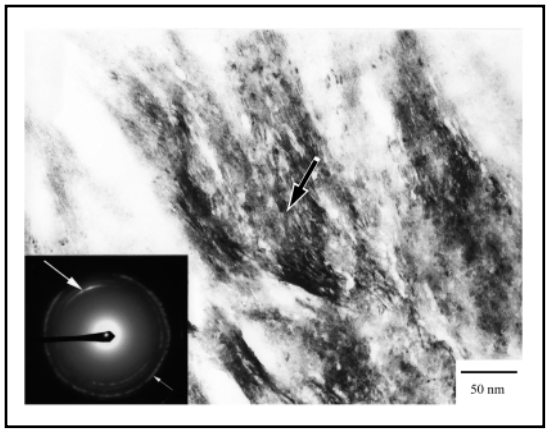

Fig.5 Bright field electron and SAD images of unstained ectopic bone cross-section prepared through the anhydrous method
A black arrow indicates the area of intrafibrillar crystallites used for the SAD image. Large and small arrows in the SAD image correspond to (002) and (211) lattice planes, respectively.

Figure 3 shows the bright field electron image of unstained cross-sections for the ectopic bone treated with the anhydrous preparation. A 64 nm well-banded feature of mineralized collagen fibril was observed even in the unstained cross-sections, due to the electron opacity of calcium phosphate. As seen in Figure 3, mineral deposits were identified in two regions, the periphery of the collagen fibrils (extrafibrillar crystallites) and the gap zone of collagen fibrils with a fine structural periodic width of 37 nm (intrafibrillar crystallites)[56-58]. Extrafibrillar crystallites appeared needle-shaped and were inclined at various angles to the long axis of the collagen fibril. On the other hand, intrafibrillar crystallites were readily apparent in the gap zones of the collagen fibrils without such a fine structural feature as that seen in the extracellular crystallites although a lesser extent of the crystallites were seen in the overlap zones of the collagen fibrils.

2)Selected area diffractograms and dark field electron imaging of unstained cross-sections

Figure 4 shows a bright field electron image of unstained cross-sections together with the SAD of extrafibrillar crystallites. Two distinct electron diffraction patterns seen in Figure 4 corresponded to the (002) and (211) lattice planes of HAp crystal and appeared ring-shaped. On the contrary, Figure 5 shows a different SAD pattern observed for the

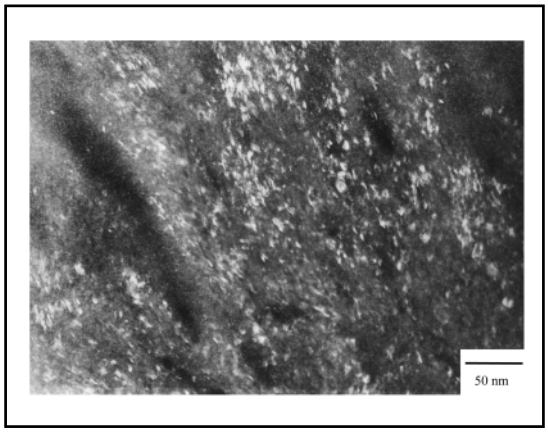

Fig.6 Dark field electron image of the c-axis of HAp crystals corresponding to the bright field electron image shown in Figure 5.

intrafibrillar crystallites, especially in the gap zones of the mineralized collagen fibril, when viewed at a higher magnification. The diffraction pattern assigned to (002) lattice plane indicated the c-axis preferential orientation of HAp crystal to the long axis of collagen fibril.

Figure 6 shows the dark field electron image of c-axis of HAp crystals corresponding to the bright field electron image shown in Figure 5. The dark field electron imaging enabled direct visualization of the HAp crystals and determination of their c-axial orientation. The dark field electron imaging appeared in reverse contrast to the conventional

bright field electron imaging with the HAp crystals appearing as white highlights. The white highlights corresponding to the c-axial diffraction of HAp crystals lay in the direction oriented to the long axis of collagen fibril, as seen in Figure 6.

Discussion

In the present study, the ultrastructure of bone tissue induced by growth factor was investigated at an electron microscopic level, in the way similar to the mineralized turkey leg tendon[35, 36, 40, 42, 43, 48-50, 52, 53]. The mineralized tendon has been widely studied as a model for mineralized tissues, such as bone and dentin. In order to minimize the artifacts in HAp crystals caused by aqueous buffer solutions, the anhydrous method[46] was used for the specimen preparation of regenerated bone and the cross-sections were not stained with any chemicals. The electron microscopically observed mineralized collagen fibril together with osteoblasts in the active form indicates that the radiopaque area of soft x-ray photographs and the calcium deposition histologically observed at the surrounding tissue of hydrogels implanted was not due to the simple calcification of hydrogels, but bone formation induced by gelatin hydrogels incorporating BMP-2. The morphological change of mineralized collagen due to the anhydrous method was not identified as shown in Figure 2. It is possible that the morphological evidence of mineralized collagen in the formed bone shown in this study may imply its intact ultrastructure.

Various models have been proposed to explain the mineralized tissue structure. For intrafibrillar crystallites, their orientation and location in collagen fibrils have been discussed. Intrafibrillar crystallites are oriented to each other within the gap zones along the whole length of the collagen fibril and to the longitudinal collagen fibril axis at an acute angle. Most of the intrafibrillar crystallites are found in the gap zones, but with increased mineralization, the crystallites in the gap zones extend into the overlap zones with or without changing the structure of the collagen fibrils. Intrafibrillar crystallites observed for the ectopic bone localized in the gap zone of the collagen fibrils, because their clear periodic width of 37 nm consists with that observed in the non-mineralized collagen (Fig.3). However, the origin of the crystallites in the overlap zones is still unclear. The SAD and the subsequent dark field electron imagings suggest that intrafibrillar crystallites could be oriented to each other and to the longitudinal axis of the collagen fibrils (Fig.5 and 6).

On the other hand, extrafibrillar crystallites do not have such a spatial orientation. The bright field electron and the subsequent SAD imagings clearly indicate that extrafibrillar crystallites observed in the ectopic bone are not oriented to the collagen fibril axis as seen in the intrafibrillar crystallites (Fig.4). This feature consists with that observed for the mineralized turkey leg tendon. However, detailed information on the needle-shaped extrafibrillar crystallites of ectopic bone was not obtained from Figure 4. Extrafibrillar crystallites of mineralized tissues have been investigated in terms of their shape and their exact location of crystal nucleation, although needle-like appearing has not been demonstrated whether it may be their intact shape or the shape viewing on the edge of the platelet crystallites.

Not only collagen-mineral interaction, but also the orientation of mineralized collagen fibrils has been demonstrated to explain the mechanically efficient composite structure of mineralized tissues[15, 46, 45, 50, 53, 59]. In addition, a fracture-healing model has been studied on the basis of external periosteal callus of repaired femoral fractures in both children and adults to understand the mechanism of bone repair and regeneration[37, 38]. When compared with the spatial orientation of collagen fibrils observed in the fracture callus, well-ordered collagen fibrils, approximately parallel to each other and to columns of the mineral HAp, appeared in the lamellar bone. From this viewpoint, collagen fibril orientation also seems to be important with respect to the mechanical compatibility of the ectopic bone. However, as shown in this study, the preferred orientation of collagen fibrils is still unclear. Combination of the information obtained from x-ray diffraction and scanning electron microscopy with the results shown in the present study will be helpful to understand the ultrastructure of the regenerated bone.

Source of Fundind, Conflict of Interests

No potential conflicts of interest were disclosed.

References

1) An introduction to bioceramics. (eds.Hench LL, Wilson J), World Scientific, Singapore; 1993.
2) Amini AR, Laurencin CT, Nukavarapu SP: Bone tissue engineering: recent advances and challenges. Crit Rev Biomed Eng. 2012; 40: 363-408.

3) Mehta M, Schmidt-Bleek K, Duda GN, Mooney DJ: Biomaterial delivery of morphogens to mimic the natural healing cascade in bone. Adv Drug Deliv Rev. 2012; 64: 1257-1276.
4) Vo TN, Kasper FK, Mikos AG: Strategies for controlled delivery of growth factors and cells for bone regeneration. Adv Drug Deliv Rev. 2012; 64: 1292-1309.
5) King WJ, Krebsbach PH: Growth factor delivery: How surface interactions modulate release in vitro and in vivo. Adv Drug Deliv Rev. 2012; 64: 1239-1256.
6) Tabata Y: Biomaterial technology for tissue engineering applications. J R Soc Interface. 2009; 6: S311-S324.
7) Takahashi Y, Yamamoto M, Yamada K, Kawakami O, Tabata Y: Skull bone regeneration in nonhuman primates by controlled release of bone morphogenetic protein-2 from a biodegradable hydrogel. Tissue Eng. 2007; 13: 293-300.
8) Yamamoto M, Takahashi Y, Tabata Y: Enhanced bone regeneration at a segmental bone defect by controlled release of bone morphogenetic protein-2 from a biodegradable hydrogel. Tissue Eng. 2006; 12: 1305-1311.
9) Yamamoto M, Takahashi Y, Tabata Y: Controlled release by biodegradable hydrogels enhances the ectopic bone formation of bone morphogenetic protein. Biomaterials. 2003; 24: 4375-4383.
10) Nakano T, Kaibara K, Tabata Y, Nagata N, Enomoto S, Marukawa E, et al: Unique alignment and texture of biological apatite crystallites in typical calcified tissues analyzed by microbeam X-ray diffractometer system. Bone. 2002; 31: 479-487.
11) Nightingale JP, Lewis D: Pole figures of the orientation of apatite in bones. Nature. 1971; 232: 334-335.
12) Sasaki N, Sudoh Y: X-ray pole figure analysis of apatite crystals and collagen molecules in bone. Calcified Tissue Int. 1997; 60: 361-367.
13) Sasaki N, Matsushima N, Ikawa T, Yamamura H, Fukuda A: Orientation of Bone-Mineral and Its Role in the Anisotropic Mechanical-Properties of Bone - Transverse Anisotropy. J Biomech. 1989; 22: 157-164.
14) Fratzl P, Fratzlzelman N, Klaushofer K, Vogl G, Koller K: Nucleation and Growth of Mineral Crystals in Bone Studied by Small-Angle X-Ray-Scattering. Calcified Tissue Int. 1991; 48: 407-413.
15) Fratzl P, Paris O, Klaushofer K, Landis WJ: Bone mineralization in an osteogenesis imperfecta mouse model studied by small-angle x-ray scattering. J Clin Invest. 1996; 97: 396-402.
16) Fratzl P, Schreiber S, Klaushofer K: Bone mineralization as studied by small-angle x-ray scattering. Connect Tissue Res. 1996; 35: 9-16.
17) Bacon GE, Goodship AE: The Orientation of the Mineral Crystals in the Radius and Tibia of the Sheep, and Its Variation with Age. J Anat. 1991; 179: 15-22.
18) Bacon GE, Griffiths RK: Texture, Stress and Age in the Human Femur. J Anat. 1985; 143: 97-101.
19) Wenk HR, Heidelbach F: Crystal alignment of carbonated apatite in bone and calcified tendon: Results from quantitative texture analysis. Bone. 1999; 24: 361-369.
20) Gourion-Arsiquaud S, Allen MR, Burr DB, Vashishth D, Tang SY, Boskey AL: Bisphosphonate treatment modifies canine bone mineral and matrix properties and their heterogeneity. Bone. 2010; 46: 666-672.
21) Gourion-Arsiquaud S, Faibish D, Myers E, Spevak L, Compston J, Hodsman A, et al: Use of FTIR Spectroscopic Imaging to Identify Parameters Associated With Fragility Fracture. J Bone Miner Res. 2009; 24: 1565-1571.
22) Yerramshetty JS, Akkus O: The associations between mineral crystallinity and the mechanical properties of human cortical bone. Bone. 2008; 42: 476-482.
23) Akkus O, Adar F, Schaffler MB: Age-related changes in physicochemical properties of mineral crystals are related to impaired mechanical function of cortical bone. Bone. 2004; 34: 443-453.
24) Boyde A, Riggs CM: The Quantitative Study of the Orientation of Collagen in Compact-Bone Slices. Bone. 1990; 11: 35-39.
25) Goldman HM, Bromage TG, Thomas CDL, Bruns R, Clement JG: Preferred collagen fiber orientation in the human mid-shaft femur. Anat Rec. 2003; 272A: 435-445.
26) Janko M, Davydovskaya P, Bauer M, Zink A, Stark RW: Anisotropic Raman scattering in collagen bundles. Opt Lett. 2010; 35: 2765-2767.
27) Nakano T, Kaibara K, Ishimoto T, Tabata Y, Umakoshi Y: Biological apatite (BAp) crystallographic orientation and texture as a new index for assessing the microstructure and function of bone regenerated by tissue engineering. Bone. 2012; 51: 741-747.
28) Nakano T, Kaibara K, Tabata Y, Nagata N, Enomoto S, Marukawa E, et al: Analysis of hydroxyapatite (HAp) texture in regenerated hard tissues using micro-beam

X-ray diffractometer technique; Tissue engineering for therapeutic use 6. (eds. Ikada Y, Umakoshi Y, Hotta T), Excerpta Medica, Tokyo; 2002, pp95-104.

29) Umakoshi Y, Nakano T, Ishimoto T, Tabata Y, Yamamoto M: Role of stress distribution on healing process of preferential alignment of biological apatite in long bones; Mater Sci Forum Vol.512. (eds Umakoshi Y, Fujimoto S), Trans Tech Publ, Dürnten, Switzerland; 2006, pp261-264.

30) Ishimoto T, Nakano T, Umakoshi Y, Yamamoto M, Tabata Y: Degree of biological apatite c-axis orientation rather than bone mineral density controls mechanical function in bone regenerated using recombinant bone morphogenetic protein-2. J Bone Miner Res. 2013; 28: 1170-1179.

31) Ishimoto T, Nakano T, Yamamoto M, Tabata Y: Biomechanical evaluation of regenerating long bone by nanoindentation. J Mater Sci-Mater Med. 2011; 22: 969-976.

32) Plate U, Arnold S, Reimer L, Hohling HJ, Boyde A: Investigation of the Early Mineralization on Collagen in Dentin of Rat Incisors by Quantitative Electron Spectroscopic Diffraction (Esd). Cell Tissue Res. 1994; 278: 543-547.

33) Bonucci E: Ultrastructural organic-inorganic relationships in calcified tissues: Cartilage and bone vs enamel. Connect Tissue Res. 1995; 32: 479-484.

34) Hohling HJ, Arnold S, Barckhaus RH, Plate U, Wiesmann HP: Structural relationship between the primary crystal formations and the matrix macromolecules in different hard tissues. Discussion of a general principle. Connect Tissue Res. 1995; 32: 493-500.

35) Lees S, Prostak KS, Ingle VK, Kjoller K: The loci of mineral in turkey leg tendon as seen by atomic force microscope and electron microscopy. Calcif Tissue Int. 1994; 55: 180-189.

36) Prostak KS, Lees S: Visualization of crystal-matrix structure. In situ demineralization of mineralized turkey leg tendon and bone. Calcif Tissue Int. 1996; 59: 474-479.

37) Wen HB, Cui FZ, Feng QL, Li HD, Zhu XD: Microstructural Investigation of the Early External Callus after Diaphyseal Fractures of Human Long-Bone. J Struct Biol. 1995; 114: 115-122.

38) Cui FZ, Wen HB, Su XW, Zhu XD: Microstructures of external periosteal callus of repaired femoral fracture in children. J Struct Biol. 1996; 117: 204-208.

39) Arsenault AL, Hunziker EB: Electron-Microscopic Analysis of Mineral-Deposits in the Calcifying Epiphyseal Growth Plate. Calcified Tissue Int. 1988; 42: 119-126.

40) Arsenault AL: Crystal-Collagen Relationships in Calcified Turkey Leg Tendons Visualized by Selected-Area Dark Field Electron-Microscopy. Calcified Tissue Int. 1988; 43: 202-212.

41) Arsenault AL, Grynpas MD: Crystals in Calcified Epiphyseal Cartilage and Cortical Bone of the Rat. Calcified Tissue Int. 1988; 43: 219-225.

42) Arsenault AL: Image-Analysis of Collagen-Associated Mineral Distribution in Cryogenically Prepared Turkey Leg Tendons. Calcified Tissue Int. 1991; 48: 56-62.

43) Arsenault AL, Frankland BW, Ottensmeyer FP: Vectorial Sequence of Mineralization in the Turkey Leg Tendon Determined by Electron-Microscopic Imaging. Calcified Tissue Int. 1991; 48: 46-55.

44) Giraudguille MM: Twisted Plywood Architecture of Collagen Fibrils in Human Compact-Bone Osteons. Calcified Tissue Int. 1988; 42: 167-80.

45) Isaac D, Green M: The origins of preferred orientation in bone. Clin Mater. 1994; 15: 79-87.

46) Landis WJ, Paine MC, Glimcher MJ: Electron-Microscopic Observations of Bone Tissue Prepared Anhydrously in Organic-Solvents. J Ultra Mol Struct Res. 1977; 59: 1-30.

47) Ziv V, Sabanay I, Arad T, Traub W, Weiner S: Transitional structures in lamellar bone. Microsc Res Techniq. 1996; 33: 203-213.

48) Kohler DM, Crenshaw MA, Arsenault AL: 3-Dimensional Analysis of Mineralizing Turkey Leg Tendon Matrix Vesicle Collagen Relationships. Matrix Biol. 1995; 14: 543-552.

49) Landis WJ, Song MJ, Leith A, Mcewen L, Mcewen BF: Mineral and Organic Matrix Interaction in Normally Calcifying Tendon Visualized in 3 Dimensions by High-Voltage Electron-Microscopic Tomography and Graphic Image-Reconstruction. J Struct Biol. 1993; 110: 39-54.

50) Landis WJ: The Strength of a Calcified Tissue Depends in Part on the Molecular-Structure and Organization of Its Constituent Mineral Crystals in Their Organic Matrix. Bone. 1995; 16: 533-544.

51) Landis WJ, Hodgens KJ, Arena J, Song MJ, McEwen

BF: Structural relations between collagen and mineral in bone as determined by high voltage electron microscopic tomography. Microsc Res Techniq. 1996; 33: 192-202.

52) Landis WJ, Hodgens KJ, Song MJ, Arena J, Kiyonaga S, Marko M, et al: Mineralization of collagen may occur on fibril surfaces: Evidence from conventional and high-voltage electron microscopy and three-dimensional imaging. J Struct Biol. 1996; 117: 24-35.

53) Landis WJ: Mineral characterization in calcifying tissues: Atomic, molecular and macromolecular perspectives. Connect Tissue Res. 1996; 35: 1-8.

54) Riminucci M, Silvestrini G, Bonucci E, Fisher LW, Robey PG, Bianco P: The Anatomy of Bone Sialoprotein Immunoreactive Sites in Bone as Revealed by Combined Ultrastructural Histochemistry and Immunohistochemistry. Calcified Tissue Int. 1995; 57: 277-284.

55) McKee MD, Nanci A: Osteopontin at mineralized tissue interfaces in bone, teeth, and osseointegrated implants: Ultrastructural distribution and implications for mineralized tissue formation, turnover, and repair. Microsc Res Techniq. 1996; 33: 141-164.

56) Chapman JA: The staining pattern of collagen fibrils. I. An analysis of electron micrographs. Connect Tissue Res. 1974; 2: 137-150.

57) Chapman JA, Hardcastle RA: The staining pattern of collagen fibrils. II. A comparison with patterns computer-generated from the amino acid sequence. Connect Tissue Res. 1974; 2: 151-159.

58) Meek KM, Chapman JA, Hardcastle RA: The staining pattern of collagen fibrils. Improved correlation with sequence data. J Biol Chem. 1979; 254: 10710-10714.

59) Landis WJ, Librizzi JJ, Dunn MG, Silver FH: A Study of the Relationship between Mineral-Content and Mechanical-Properties of Turkey Gastrocnemius Tendon. J Bone Miner Res. 1995; 10: 859-867.